

© 2021 IEEE. Personal use of this material is permitted. Permission from IEEE must be obtained for all other uses, in any current or future media, including reprinting/republishing this material for advertising or promotional purposes, creating new collective works, for resale or redistribution to servers or lists, or reuse of any copyrighted component of this work in other works.

A LIGHTWEIGHT RELU-BASED FEATURE FUSION FOR AERIAL SCENE CLASSIFICATION

Md Adnan Arefeen* Sumaiya Tabassum Nimi* Md Yusuf Sarwar Uddin* Zhu Li*

* Department of EECS, University of Missouri-Kansas City, MO, USA

ABSTRACT

In this paper, we propose a transfer-learning based model construction technique for the aerial scene classification problem. The core of our technique is a layer selection strategy, named ReLU-Based Feature Fusion (RBFF), that extracts feature maps from a pretrained CNN-based single-object image classification model, namely MobileNetV2, and constructs a model for the aerial scene classification task. RBFF stacks features extracted from the batch normalization layer of a few selected blocks of MobileNetV2, where the candidate blocks are selected based on the characteristics of the ReLU activation layers present in those blocks. The feature vector is then compressed into a low-dimensional feature space using dimension reduction algorithms on which we train a low-cost SVM classifier for the classification of the aerial images. We validate our choice of selected features based on the significance of the extracted features with respect to our classification pipeline. RBFF remarkably does not involve any training of the base CNN model except for a few parameters for the classifier, which makes the technique very cost-effective for practical deployments. The constructed model despite being lightweight outperforms several recently proposed models in terms of accuracy for a number of aerial scene datasets.

Index Terms— Layer selection, Aerial image analysis, Transfer learning, Feature fusion, Image classification

1. INTRODUCTION

Aerial image classification involves categorizing aerial images into an exhaustive set of known classes based on the contents of the images. In recent years, several research works have been conducted to classify remote sensing images because of its application in the military and civil tasks such as disaster management [1], traffic supervision [2], environmental monitoring [3] and urban mapping [4]. The earliest efforts towards aerial image classification employed

pixel-level and object-level analysis approaches [5]. In the recent years, deep learning models such as Convolutional Neural Networks (CNN) have emerged as one of the best tools for computer vision tasks like image classification and face recognition. Consequently, CNN models have been applied for aerial image classification also, leading to better classification performance compared to the prior approaches. Most

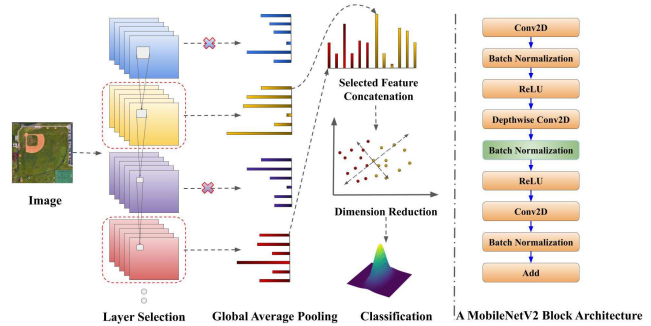


Fig. 1: ReLU-Based Feature Fusion in MobileNetV2 Block Architecture

of the research works that employ CNN based approaches for the task of remote scene classification train the CNN model from scratch on the pertinent dataset [6, 7, 8]. The training phase involved in these approaches is computationally very expensive.

In the current work, we propose a transfer learning-based methodology for the same task (i.e., remote scene classification) that *does not* require training of any CNN model. Our proposed approach, ReLU-Based Feature Fusion (RBFF), involves stacking features extracted from batch normalization layers of a few *selected* blocks based on a layer significance value from the lightweight MobileNetV2 [9] model pretrained on ImageNet [10] dataset. A block of MobileNetV2 with the proposed pipeline is depicted in Figure 1. Before concatenating the extracted features, we use the global con-

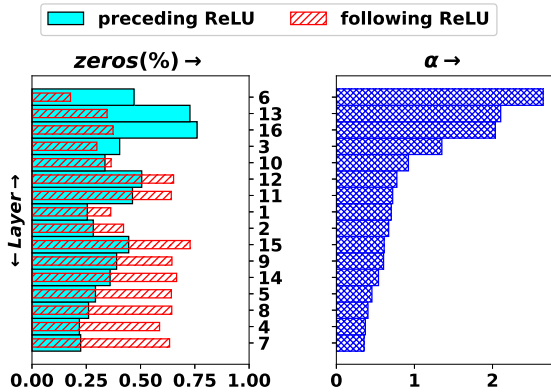


Fig. 2: Zero percentage for the preceding ReLU layer and the following ReLU layer for each layer of AID dataset (left). The layers are sorted according to highest value of α (right).

text of the features which helps reducing the dimension of the feature maps without eliminating the global context of the features. We further compress the features using dimension reduction techniques such as Principal Component Analysis (PCA) [11] and Linear Discriminant Analysis (LDA) [12] so that we get a more compact low-dimensional feature space without major loss of information. Finally, we use a one-vs-rest support vector machine (SVM) model on the compressed feature space for classification of the aerial images. The cost-effectiveness of our proposed model is two-fold. The model is space-efficient as its size is very small compared to the deep learning models that have been proposed so far for the task of remote scene classification (3.28 ~ 13.28 MB). Furthermore, we investigate the accuracy vs model size trade-off issue as our technique employs two dimension reduction techniques in the pipeline, which comes with additional overhead in terms of the overall model size.

2. BACKGROUND AND MOTIVATION

We have used pretrained lightweight MobilenetV2 model to extract the deep features through a layer selection strategy (RBFF), Whereas in [13], a nonparametric self-attention layer is proposed to get the more discriminative features from the pretrained CNN model (VGG-VD16 [14] and AlexNet [15]). In [16], novel loss function was proposed so that the feature space of the deep learning model learned on the objective would discern between images representing separate classes, so that features of the images belonging to the same class would be mapped closer in the learned feature space and vice-versa for images belonging to different classes. Meanwhile, in [17], texture information of images obtained using Local Binary Pattern (LBP) was used in addition to traditional RGB images for training deep learning models. On the contrary, in [8], a novel network architecture was proposed for aerial image classification, that consisted of dense blocks with addi-

tion and modification of residual attention layers and a classification layer. The network was designed to contain fewer parameters than the traditional models. Traditional VGGNet architecture was modified in [18] to incorporate local and global attention layers in order to capture the corresponding information from aerial images, along with subsidiary objectives added to the loss function for additional supervision.

Contrary to all these approaches, our proposed method is free from the huge overhead of deep learning model training. To classify aerial images, we follow a layer selection based transfer learning based approach where we apply a novel technique to select the most informative layers from a pretrained model.

3. METHODS

3.1. ReLU-Based Feature Fusion

The most trivial approach can be the extraction of features from each layer which will result in accumulating a large number of features for a single image. Hence, rather than extracting features from each layer, we intuitively choose a subset of layers from the MobileNetV2 architecture for feature extraction. In MobileNetV2 [9], each block architecture is of ReLU \circ Conv \circ BN \circ ReLU like fashion. There are 16 of such blocks in MobileNetV2. One such block is depicted in Figure 1. The BN layer within a block is surrounded by two ReLU layers in the same block, which are referred to as *preceding* and *following* ReLU layers respectively with respect to that BN layer. The ReLU layers are activation layers that replace its input x to $\max(0, x)$. The ratio of the fraction of zeros in the *preceding* and *following* ReLU layers around a BN layer designates the degree of significance of the BN layer in a given block. We denote this significance by α for each block. More formally, the layer significance, α , per block is defined as:

$$\alpha = \frac{Z_{prev}}{Z_{next}}; \quad Z_{(.)} = \frac{1}{N} \sum_{i=1}^N (1 - v_i); \quad v_i = \frac{\sum_{x \in U^i} x > 0}{|U^i|}$$

where Z_{prev} and Z_{next} denote the average zero volume percentage of the preceding and the following ReLU layers of a BN layer, respectively. By zero volume, we mean how many zero elements exist in the output after a ReLU layer. If $Z_{prev} > Z_{next}$ i.e. $\alpha > 1$, the corresponding BN layer is more informative and vice versa. For an output tensor of i^{th} ReLU layer, $U^i \in \mathbb{R}^{\mathcal{H} \times \mathcal{W} \times \mathcal{C}}$, where \mathcal{H} , \mathcal{W} , and \mathcal{C} refers to height, width, and channels of the feature map, we compute positive volume percentage of i^{th} layer v_i for each input image being fed to the network. So, $(1 - v_i)$ is the zero volume percentage of a layer. To ensure minimal training, we randomly take 5 images from each class, calculate v_i of the layer for each image, and average them to get the general view of the layer. In this way, we compute the $Z_{(.)}$ for a given layer.

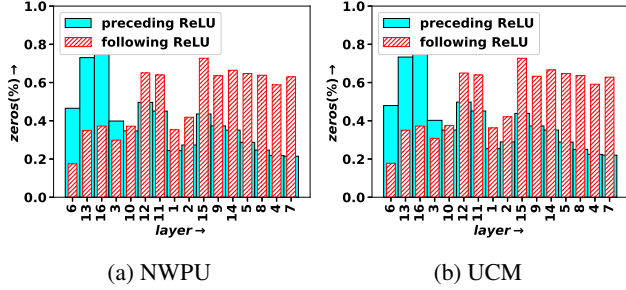


Fig. 3: Zero percentage for the preceding ReLU layer and the following ReLU layer for each block.

The average positive volume of a layer is reciprocal to the average percent of zeros in a layer in terms of α . Conceptually, α measures the importance of a batch normalization layer of each block. The higher the value of α is, the more important the batch normalization layer is in terms of its suitability to be included in the feature extraction. Consequently, we stack features from top BN layers that have higher α values. Figure 2 shows the significance of BN layers for all 16 blocks of MobilenetV2 for AID dataset. The layers are sorted with respect to higher value of α . We observe from the figure that, the top discriminative blocks are 3, 6, 13, and 16 (the blocks with higher α values for their respective BN layers). Similar characteristic is also identified for NWPU and UCM dataset in Figure 3.

Based on the α values, we stack features from the BN layers of blocks 3, 6, 13, and 16 of MobileNetV2 (these are the blocks that have the largest α values). To extract the global context information of the features from the selected layers, we apply the global attention based feature extraction. The global average pooling (GAP) [19] is used to achieve this. For a channel c of i^{th} layer feature map, U_c^i the global average pooling will be,

$$GAP(U_c^i) = \frac{1}{H \times W} \sum_{j=1}^H \sum_{k=1}^W u_c^i[j, k] \quad (1)$$

For each channel the 2-D $H \times W$ feature map is converted to one value. Thus, global average pooling captures the global information of each channel of a layer output by converting 3-D tensor to a series of vector. By this way, a global attention based feature map is achieved.

3.2. Batch Normalization Layer in the Context of LDA

Batch normalization repeatedly enforces the activations to have zero mean and unit standard deviation [20], leading to faster and optimal convergence of the neural network training. In our approach, we use this fact to our advantage. Prior to the SVM classification, we use LDA for dimension reduction. Since LDA works best for normally distributed data, our choice of using the feature maps from the BN layers leads

Table 1: Description of Datasets

Dataset	Number of Classes	Number of Samples per Class
UCM	21	100
AID	30	220-400
NWPU	45	700

Table 2: Model Parameters and Feature Dimension

Model	Parameters (in Millions)	Model Size (in MB)	Feature Dimension
AlexNet [22]	60	434	4096
VGG-VD-16 [22]	138	1024	4096
GoogLeNet [22]	6.8	91.1	1024
RADC-Net [8]	0.5	9.0	352
MIDC-Net_CS [7]	0.5	10.0	-
RBFF (3.6_13_16)	1.46	6.28	1872
RBFF (3.6_13)	0.59	2.73	912
RBFF + PCA + LDA + SVM	-	3.28~13.28	$k - 1$

to the optimal performance of LDA and hence the optimal classification of the aerial images.

4. RESULTS

4.1. Datasets

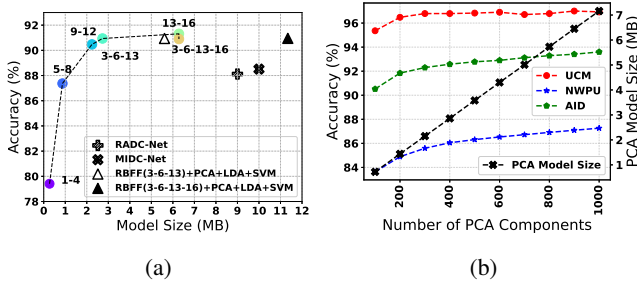
In this paper, we have used three widely used aerial scene datasets, namely UCM [21], AID [22], NWPU [23]. The description of these datasets in terms of the number of classes and the number of samples per class is listed in Table 1.

4.2. Experimental Settings

We consider the BN layers of the top 3 and 4 blocks among 16 blocks in the descending order of their α values as evident from Figure 2. After the feature extraction phase, we successively perform GAP, PCA, LDA, and SVM on the features and report the classification results using cross-validation technique. The size of the actual MobileNetV2 model is approximately 14 MB. After transfer learning using our proposed RBFF technique, the model size is reduced to 6.28 MB as shown in Table 2. Excluding the last layer (layer 16) from RBFF, the size is only 2.73 MB. In Table 2, k means the number of classes as after LDA, the features are reduced to only number of classes minus one if explicit reduction is not provided to the LDA model. We choose 600 as the number of components for PCA. The reason is discussed in section 4.4. We also show results without PCA to perform the ablation study. The detail is discussed in section 4.5. These experiments are done under a fixed random state for PCA, RepeatedStratified K-Fold, and SVM. The random states are 3, 33, and 333 respectively for PCA, RepeatedStratified K-Fold, and SVM to reproduce the results. We have used the `scikit-learn` package [26] to implement these algorithms. Our experiments have been done on NVIDIA Quadro RTX 4000 GPU and i7-9750 CPU@2.60GHz.

Table 3: Accuracy comparison of RBFF with Different Methods for Different Datasets

Method	AID (20%)	AID (50%)	NWPU (10%)	NWPU (20%)	UCM (50%)	UCM (80%)
PLSA (SIFT) [22]	56.24 ± 0.58	63.07 ± 1.77	–	–	67.55 ± 1.11	71.38 ± 1.77
BoVW (SIFT) [22]	62.49 ± 0.53	68.37 ± 0.40	41.72 ± 0.21	44.97 ± 0.28	73.48 ± 1.39	75.52 ± 2.13
LDA (SIFT) [22]	51.73 ± 0.73	68.96 ± 0.58	–	–	59.24 ± 1.66	75.98 ± 1.60
AlexNet [22]	86.86 ± 0.47	89.53 ± 0.31	76.69 ± 0.21	79.85 ± 0.13	93.98 ± 0.67	95.02 ± 0.81
VGGNet-16 [22]	86.59 ± 0.29	89.64 ± 0.36	76.47 ± 0.18	79.79 ± 0.15	94.14 ± 0.69	95.21 ± 1.20
GoogLeNet [22]	83.44 ± 0.40	86.39 ± 0.55	76.19 ± 0.38	78.48 ± 0.26	92.70 ± 0.60	94.31 ± 0.89
SPP with Alexnet [24]	87.44 ± 0.45	91.45 ± 0.38	82.13 ± 0.30	84.64 ± 0.23	94.77 ± 0.46	96.67 ± 0.94
D-CNN with AlexNet [16]	85.62 ± 0.10	94.47 ± 0.12	85.56 ± 0.20	87.24 ± 0.12	–	96.67 ± 0.10
TEX-Net with VGG [17]	87.32 ± 0.37	90.00 ± 0.33	–	–	94.22 ± 0.50	95.31 ± 0.69
Gated Attention [25]	87.63 ± 0.44	92.01 ± 0.21	84.94 ± 0.22	86.62 ± 0.22	94.64 ± 0.43	96.12 ± 0.42
MIDC-Net_CS [7]	88.51 ± 0.41	92.95 ± 0.17	86.12 ± 0.29	87.99 ± 0.18	95.41 ± 0.40	97.40 ± 0.48
RADC-Net [8]	88.12 ± 0.43	92.35 ± 0.19	85.72 ± 0.25	87.63 ± 0.28	94.79 ± 0.42	97.05 ± 0.48
VGG_VD16 + SAFF [13]	90.25 ± 0.29	93.83 ± 0.28	84.38 ± 0.19	87.86 ± 0.14	–	97.02 ± 0.78
RBFF (3_6_13) + PCA (600) + LDA + SVM	90.94 ± 0.26	93.73 ± 0.23	84.59 ± 0.24	87.53 ± 0.19	94.69 ± 0.34	96.40 ± 0.99
RBFF (3_6_13_16) + PCA (600) + LDA + SVM	91.02 ± 0.22	92.90 ± 0.31	84.24 ± 0.29	86.53 ± 0.20	95.83 ± 0.54	96.90 ± 1.14
RBFF (3_6_13) + LDA + SVM	–	93.64 ± 0.42	–	87.5 ± 0.24	–	94.93 ± 0.82
RBFF (3_6_13_16) + LDA + SVM	–	93.64 ± 0.48	–	88.05 ± 0.18	–	82.38 ± 1.92

**Fig. 4:** (a) Comparison of sorted mean accuracy with total model size for the same dataset (AID (20%)) and same configuration. (b) Accuracy, model size and the number of PCA components for all three datasets used in this paper.

4.3. Experimental Analysis

We compare our approach with some recently proposed network architectures in terms of classification accuracy. Table 3 represents the overall accuracy results for three datasets. The AID and NWPU datasets are comparatively harder to classify than the UCM dataset. During experimentation, the images are resized to 224×224 and preprocessed using the predefined `preprocess_input` function of MobileNetV2 application of Keras for ImageNet dataset. For AID with 20% training dataset, our proposed approach outperforms all the state-of-the-art results. With regard to the 50% training set, D-CNN with Alexnet outperforms all the results. RBFF holds the second best result. For 20% training set of the NWPU dataset and 50% for UCM, RBFF outperforms all recent works. For other cases, RBFF is only less than 0.5 – 1.53% than the best results.

4.4. Model size vs Accuracy

In Figure 4a, we show the superiority of RBFF to other lightweight models [7, 8]. To examine how the model size

Table 4: Comparison of Accuracy with Layer selection

Layer	Accuracy	Feature Dimension
9_10_11	92.18 ± 0.27	1344
9_10_12	92.81 ± 0.39	1344
10_11_12	92.48 ± 0.13	1536
9_11_12	92.37 ± 0.33	1536
3_6_13 (Ours)	93.64 ± 0.42	912

Table 5: Layer selection vs Accuracy trade-off

Dataset	Layer 3	Layer 6	Layer 13	Layer 16	Accuracy
NWPU	✓	✗	✗	✗	71.56 ± 0.31
NWPU	✓	✓	✗	✗	78.44 ± 0.22
NWPU	✓	✓	✓	✗	87.5 ± 0.24
NWPU	✓	✓	✓	✓	88.05 ± 0.18
AID	✓	✗	✗	✗	82.07 ± 0.88
AID	✓	✓	✗	✗	87.85 ± 0.56
AID	✓	✓	✓	✗	93.64 ± 0.42
AID	✓	✓	✓	✓	93.64 ± 0.48

changes if we choose different depthwise BN layers, we divide the 16 selected BN layers into four chunks, namely 1–4, 5–8, 9–12, and 13–16 and observe accuracy vs model size (Figure 4a). As layers 9–12 exhibit similar performance compared our proposed RBFF, we compare the 3–6–13 with each three combinations from 9–12 for AID (50% training) in Table 4 where RBFF has a lower cost with higher accuracy. The increase of the PCA model size with the increase of PCA components is illustrated in Figure 4b. Based on Figure 4b, we have chosen 600 components for PCA for having higher accuracy and comparatively lower PCA model size. One can use this hyperparameter as a knob to fit when necessary.

4.5. Ablation Study

To show the effect of layer selection on accuracy, we add a layer from our selection algorithm from the top layer to the

deeper layer. We observe an increase in accuracy in most of the cases. We experimented this with AID (50% training) and NWPU (20% training) datasets as shown in Table 5 using only LDA for dimension reduction and SVM for classification as the feature dimension changes every time. The result demonstrates the significance of our layer selection.

5. CONCLUSION

In this paper, we have proposed a novel approach for the classification of aerial images that extracts and fuses features from selected layers of the pretrained MobileNetV2 model based on feature fusion strategy. We have shown that our constructed model achieves similar or superior classification accuracy although the size of the model is smaller compared to the earlier works and the training cost is very minimal. While we apply the ReLU-based feature fusion on MobileNetV2 for only the aerial scene classification, we recognize that the technique can be applied on other transfer learning tasks too. In the future, we intend to investigate further on this.

6. REFERENCES

- [1] Christos Kyrkou and Theodoris Theodoridis, "Deep-learning-based aerial image classification for emergency response applications using unmanned aerial vehicles.," in *CVPR Workshops*, 2019, pp. 517–525.
- [2] Yohei Koga, Hiroyuki Miyazaki, and Ryosuke Shibasaki, "A cnn-based method of vehicle detection from aerial images using hard example mining," *remote sensing*, vol. 10, no. 1, pp. 124, 2018.
- [3] Shengke Wang, Lu Liu, Liang Qu, Changyin Yu, Yujuan Sun, Feng Gao, and Junyu Dong, "Accurate ulva prolifera regions extraction of uav images with superpixel and cnns for ocean environment monitoring," *Neurocomputing*, vol. 348, pp. 158–168, 2019.
- [4] Hao Wu, Hanyuan Zhang, Xinyu Zhang, Weiwei Sun, Baihua Zheng, and Yuning Jiang, "Deepdualmapper: A gated fusion network for automatic map extraction using aerial images and trajectories," in *Proceedings of the AAAI Conference on Artificial Intelligence*, 2020, vol. 34, pp. 1037–1045.
- [5] Gong Cheng, Junwei Han, Lei Guo, Zhenbao Liu, Shuhui Bu, and Jinchang Ren, "Effective and efficient midlevel visual elements-oriented land-use classification using vhr remote sensing images," *IEEE Transactions on Geoscience and Remote Sensing*, vol. 53, no. 8, pp. 4238–4249, 2015.
- [6] Miaohui Zhang, Kangning Pang, Chengcheng Gao, and Ming Xin, "Multi-scale aerial target detection based on densely connected inception resnet," *IEEE Access*, vol. 8, pp. 84867–84878, 2020.
- [7] Qi Bi, Kun Qin, Zhili Li, Han Zhang, Kai Xu, and Gui-Song Xia, "A multiple-instance densely-connected convnet for aerial scene classification," *IEEE Transactions on Image Processing*, vol. 29, pp. 4911–4926, 2020.
- [8] Qi Bi, Kun Qin, Han Zhang, Zhili Li, and Kai Xu, "Radc-net: A residual attention based convolution network for aerial scene classification," *Neurocomputing*, vol. 377, pp. 345–359, 2020.
- [9] Mark Sandler, Andrew Howard, Menglong Zhu, Andrey Zhmoginov, and Liang-Chieh Chen, "Mobilenetv2: Inverted residuals and linear bottlenecks," in *Proceedings of the IEEE conference on computer vision and pattern recognition*, 2018, pp. 4510–4520.
- [10] J. Deng, W. Dong, R. Socher, L.-J. Li, K. Li, and L. Fei-Fei, "ImageNet: A Large-Scale Hierarchical Image Database," in *CVPR09*, 2009.
- [11] Svante Wold, Kim Esbensen, and Paul Geladi, "Principal component analysis," *Chemometrics and intelligent laboratory systems*, vol. 2, no. 1-3, pp. 37–52, 1987.
- [12] Peter A Lachenbruch and M Goldstein, "Discriminant analysis," *Biometrics*, pp. 69–85, 1979.
- [13] Ran Cao, Leyuan Fang, Ting Lu, and Nanjun He, "Self-attention-based deep feature fusion for remote sensing scene classification," *IEEE Geoscience and Remote Sensing Letters*, 2020.
- [14] Alex Krizhevsky, Ilya Sutskever, and Geoffrey E Hinton, "Imagenet classification with deep convolutional neural networks," in *Advances in neural information processing systems*, 2012, pp. 1097–1105.
- [15] Karen Simonyan and Andrew Zisserman, "Very deep convolutional networks for large-scale image recognition," *arXiv preprint arXiv:1409.1556*, 2014.
- [16] Gong Cheng, Ceyuan Yang, Xiwen Yao, Lei Guo, and Junwei Han, "When deep learning meets metric learning: Remote sensing image scene classification via learning discriminative cnns," *IEEE transactions on geoscience and remote sensing*, vol. 56, no. 5, pp. 2811–2821, 2018.
- [17] Rao Muhammad Anwer, Fahad Shahbaz Khan, Joost van de Weijer, Matthieu Molinier, and Jorma Laaksanen, "Binary patterns encoded convolutional neural networks for texture recognition and remote sensing scene classification," *ISPRS journal of photogrammetry and remote sensing*, vol. 138, pp. 74–85, 2018.
- [18] Yiyu Guo, Jinsheng Ji, Xiankai Lu, Hong Huo, Tao Fang, and Deren Li, "Global-local attention network for aerial scene classification," *IEEE Access*, vol. 7, pp. 67200–67212, 2019.
- [19] Min Lin, Qiang Chen, and Shuicheng Yan, "Network in network," *arXiv preprint arXiv:1312.4400*, 2013.
- [20] Nils Bjorck, Carla P Gomes, Bart Selman, and Kilian Q Weinberger, "Understanding batch normalization," in *Advances in Neural Information Processing Systems*, 2018, pp. 7694–7705.
- [21] Yi Yang and Shawn Newsam, "Geographic image retrieval using local invariant features," *IEEE Transactions on Geoscience and Remote Sensing*, vol. 51, no. 2, pp. 818–832, 2012.
- [22] Gui-Song Xia, Jingwen Hu, Fan Hu, Baoguang Shi, Xiang Bai, Yanfei Zhong, Liangpei Zhang, and Xiaoqiang Lu, "Aid: A benchmark data set for performance evaluation of aerial scene classification," *IEEE Transactions on Geoscience and Remote Sensing*, vol. 55, no. 7, pp. 3965–3981, 2017.
- [23] Gong Cheng, Junwei Han, and Xiaoqiang Lu, "Remote sensing image scene classification: Benchmark and state of the art," *Proceedings of the IEEE*, vol. 105, no. 10, pp. 1865–1883, 2017.

- [24] Xiaobing Han, Yanfei Zhong, Liqin Cao, and Liangpei Zhang, "Pre-trained alexnet architecture with pyramid pooling and supervision for high spatial resolution remote sensing image scene classification," *Remote Sensing*, vol. 9, no. 8, pp. 848, 2017.
- [25] Maximilian Ilse, Jakub Tomczak, and Max Welling, "Attention-based deep multiple instance learning," in *Proceedings of the 35th International Conference on Machine Learning*, Jennifer Dy and Andreas Krause, Eds., Stockholm, Sweden, 10–15 Jul 2018, vol. 80 of *Proceedings of Machine Learning Research*, pp. 2127–2136, PMLR.
- [26] F. Pedregosa, G. Varoquaux, A. Gramfort, V. Michel, B. Thirion, O. Grisel, M. Blondel, P. Prettenhofer, R. Weiss, V. Dubourg, J. Vanderplas, A. Passos, D. Cournapeau, M. Brucher, M. Perrot, and E. Duchesnay, "Scikit-learn: Machine learning in Python," *Journal of Machine Learning Research*, vol. 12, pp. 2825–2830, 2011.